A Biosensor Based on Interchain Reactions for the Detection of Acetamiprid and the Construction of Basic Logic Gates OR and AND

Mengyang Hu, Luhui Wang, Sunfan Xi, Rong Liu, and Yafei Dong

***Abstract*— An enzyme-free and label-free fluorescent DNA aptasensor was constructed with computer assistance based on thermodynamic deviation driving interchain reactions. In this work, in the presence of target acetamiprid, the released trigger strand C-apt could open hairpin Hp1, which in turn triggered the strand displacement reaction and catalyzed the self-assembly of hairpins Hp1 and Hp2, so that the guanine base rich stem in Hp2 was opened. In the presence of K^+ and NMM, the G-rich moiety could form a G-quadruplex and emit strong fluorescence at a specific excitation wavelength. The proposed strategy enables sensitive detection of acetamiprid at concentrations as low as 54.3 pM. Most importantly, computer-assisted analysis of the thermodynamic properties of nucleic acid strands and simulation of the reaction process and conditions of the proposed model before conducting biological experiments theoretically proves this strategy feasible and may simplify subsequent biological experiments. In addition, basic molecular logic gates, including OR and AND, were constructed based on this detection principle, and simulation tests and biological experiments were performed. The final results show that this strategy can not only have some applications in the field of food safety and environmental monitoring, but also provide a certain way for the development of molecular logic computing.**

***Index Terms*— Biosensors, computer simulation, DNA strand displacement, DNA logic gates.**

I. Introduction

ACETAMIPRID, as a novel broad spectrum insecticide with low toxicity to mammals [1], has been widely used for pest control in modern agriculture [2], [3]. However, the non-standard use of acetamiprid can cause environmental pollution to reduce the production of agricultural products, fish shrimps, and so on [4], [5]; excessive use can also cause exceedance of pesticide residues in agricultural products and foods, which poses a danger to human health [6]–[8]. In addition to its acute toxicity, acetamiprid has potential long-term and chronic toxic effects, including developmental neurotoxicity, genotoxicity, and others [9]. In view of these hazards, the establishment of reliable and convenient assays for acetamiprid is essential for food safety and human health. Some of the commonly used traditional analytical detection methods include high performance liquid chromatography (HPLC) [10], gas chromatography (GC) [11], liquid chromatography (LC) [12], and enzyme-linked immunosorbent assay (ELISA) [13]. However, great efforts have been devoted to finding portable, sensitive and cost-effective detection methods because these traditional methods have some disadvantages, such as high cost, time-consuming and unstable effect. DNA biosensors have attracted attention as a kind of sensing device that can convert the presence of target DNA into a detectable electrical signal [14]. It mainly consists of two parts: a recognition element and a transducer. The recognition element senses whether or not the target DNA is contained in the detection sample through DNA interstrand or interaction with some other molecular structure; the transducer is to convert the invisible signal perceived by the recognition element into an observable recorded signal. Among them, interstrand reactions such as strand displacement amplification (SDA) [15], catalytic hairpin assembly (CHA) [16], and hybridization chain reaction (HCR) have been widely used in food, pharmaceutical, chemical, clinical trials, biomedicine, and environmental monitoring due to their enzyme free, label free, highly sensitive, and programmable properties.

Currently, the development of electronic computers is increasingly limited by hardware materials, while DNA itself has strong parallel computing power, superior information storage mechanism and stability, making it attractive as a new type of logical computing material. In 2016, Li *et al.* [17] developed a DNA nanotweeter driven by catalytic hairpin self-assembly to construct AND logic gate to detect double target microRNAs. In 2019, Gong *et al.* [18] used HCR amplification technology to design different logic gates to

Manuscript received November 9, 2021; revised December 18, 2021; accepted December 26, 2021. Date of publication December 28, 2021; date of current version July 1, 2022. This work was supported in part by the National Natural Science Foundation of China under Grant 62073207 and in part by the Natural Science Foundation of Shaanxi Province under Grant 2020JM-298. *(Corresponding author: Yafei Dong.)*

Mengyang Hu and Rong Liu are with the School of Computer Science, Shaanxi Normal University, Xi'an 710119, China (e-mail: humengyang@snnu.edu.cn; liurong@snnu.edu.cn).

Luhui Wang, Sunfan Xi, and Yafei Dong are with the College of Life Sciences, Shaanxi Normal University, Xi'an 710119, China (e-mail: wangluhui@snnu.edu.cn; xisunfan@snnu.edu.cn; dongyf@snnu.edu.cn).

Digital Object Identifier 10.1109/TNB.2021.3139079

form multi-functional sensing modules, realized the complex detection of a variety of endogenous miRNAs in different living cells, and applied computing circuits to the diagnosis of miRNA related diseases, which is of great research significance to biomedicine. In 2021, Miao and Tang [19] invented a DNA logic system for bipedal walking for miRNA diagnosis based on cascade strand displacement. Most of these are aimed at realizing multi-function detection of different targets, and do not pay attention to the calculation function. Here, we combine chain replacement and catalytic hairpin self-assembly to build a basic logic computing platform, including AND and OR, focusing on logic computing functions, so as to provide a new strategy for the construction of complex logic circuits and the development of biological computing in the future.

Combined with Watson-Crick base pairing predictability [20] and programmability of DNA logic circuits, researchers can efficiently and accurately design DNA nanomachines to accomplish a wide range of complex types of molecular computing [21]. Based on these excellent features, visual DSD(a programming language and software tool) has been designed to aid in the design of DNA machines with a variety of features to predict the feasibility of experimental principles using standard methods to simulate interstrand reactions that may occur [22]. This will greatly simplify the design and testing of DNA machines prior to subsequent experiments, thereby reducing the consumption of consumables and time.

In our work, an enzyme-free and label-free DNA biosensor based on thermodynamic deviation driving interchain reactions was constructed, and the study was carried out using a novel insecticide acetamiprid which is widely applied as an example. Once it is triggered, it will cycle to work exhibiting outstanding amplification performance. The experimental principle can also be explained from the two parts of the recognition element and the converter, in which acetamiprid acts as a target and is able to be specifically recognized by Apt in the duplex, thus releasing the trigger strand C-apt, which initiates the SDA and the assembly of hairpins Hp1 and Hp2, and the converter part consists of the G-quadruplex and N-methylmesoporphyrin IX (NMM) generated after the assembly of the catalytic hairpin [23]. The 4 guanines joined by Hoogsteen hydrogen bonds form a cyclic plane, while the latter two layers or more of the tetrads form a quadruplex by π-π stacking [24]. The G-quadruplex structure was confirmed to produce strong fluorescence in combination with organic dyes, such as NMM, and was widely applied in biosensors [24], [25]. To verify the feasibility of the principle, the simulation was performed with the visual DSD before biological experiments, and then the efficacy of our acetamiprid detection system were verified by biological experiments. Finally, based on this detection method, the basic logic OR gate and AND gate are constructed by setting different inputs, and simulation analysis is carried out to demonstrate the feasibility.

II. Materials and Methods

A. Chemicals and Materials

Acetamiprid was purchased from yuanye Bio-Technology Co., Ltd (Shanghai, China). The ssDNA used in the experiments were synthesized and further purified by JKchemicalCo., Ltd. (Beijing, China). N-methyl-mesoporphyrin IX (NMM) and SYBR Green were bought from Sangon Biotech Co., Ltd. (Shanghai, China) and stored at −20°C in the dark before use. The ultra-pure water used in our experiment was purified by a Milli-Q system (18 MΩ cm). 96-Well microplates were purchased from Lingyi Biotech Co., Ltd. (Shanghai, China).

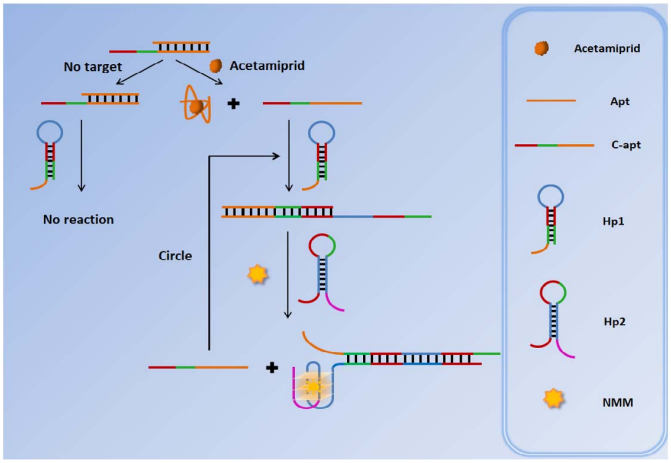

Fig. 1. The schematic illustration of acetamiprid determination using the developed fluorescent method.

B. Instrumentation

The fluorescence spectrum of NMM was measured using a fluorescence scanning spectrometer with excitation at 399 nm and emission at 610 nm through EnSpire ELIASA from PerkinElmer USA company (Shanghai, China).

C. Fluorescent Detection of Acetamiprid

Prior to experiments, the diluted solution with Hp1 (1 μM) and Hp2 (1 μM) were heated at 95°C by PCR for 5 min, and cooled to room temperature at a slow rate to form hairpin structure. And mixing C-apt (1 μM) and Apt (1.25 μM) to form a double-stranded structure. Then, different concentrations of acetamiprid, C-apt/Apt (100nM), Hp1 (300nM) and Hp2 (300nM) were mixed with the working buffer and incubated for 75 min at 35°C. After self-assembly was completed, NMM (2 μM) was added and further incubated for 25 min at 25°C. Finally, a part of the solution was removed to a 96-well plate, and the fluorescence intensity was detected and recorded by the instrument mentioned above.

III. Results and Discussion

A. Principle of Acetamiprid Detection

The schematic of this enzyme-free and label-free fluorescence detection system for acetamiprid is shown in Fig.1. This sensor contains a duplex, and two hairpins. The duplex is formed by an aptamer named Apt that can specifically bind to acetamiprid target and a single strand named C-apt complementary to it through base complementary pairing. The other two hairpins are named Hp1 and Hp2, Hp1 exists as an

intermediate auxiliary, and part of the base G-rich of Hp2 provides a fundamental factor to enable the formation of a G-quadruplex. First, if the target existed, the target would bind specifically with the aptamer Apt, thus opening the duplex structure to release the trigger strand C-apt into the next round of reaction. Next, the trigger strand opens and hybridizes with hairpin Hp1. Subsequently, strand displacement and hybridization were generated, and the binding of Hp1 and Hp2 displaced C-apt continued into the next cycle.

Strand displacement can be abstracted as (1):

$$A + B/C \rightarrow A/B + C \tag{1}$$

In the present study can be expressed as (2):

$$C - apt/Hp1 + Hp2 \rightarrow C - apt + Hp1/Hp2 \tag{2}$$

It also contains the process of hairpin self-assembly as (3):

$$Hp1 + Hp2 \rightarrow Hp1/Hp2 \tag{3}$$

To clearly delineate this reaction, trigger strand C-apt, hairpin Hp1 and hairpin Hp2 were divided into different functional fragments. As shown in illustration, the orange moiety in C-apt would open the hairpin through the binding site (orange moiety) of hairpin Hp1 and trigger the hybridization of the green and red moieties in C-apt with the green and red moieties in Hp1. Next, the generated duplex C-apt/Hp1 continues to react with Hp2, and the naked red part of the duplex opens the hairpin through the binding site (red part) of Hp2 and triggers the hybridization of the red, blue, red, and green parts in Hp2 with the corresponding fragments in the duplex. Thus, the C-apt is displaced by Hp2, resulting in a duplex structure Hp1/Hp2, in which the naked g-base-rich blue and pink moieties would form a G-quadruplex under the action of metal cations and emit strong fluorescence under the action of fluorochrome NMM, forming a positive feedback. And the displaced single stranded C-apt can trigger the next round of cycling reaction of DNA machine, so that the fluorescence is enhanced to achieve the effect of signal amplification. Thus, an enzyme-free and label-free and highly efficient strategy for the detection of acetamiprid was proposed.

B. Sequence Design and Analysis

The uniqueness of DNA is determined by the sequence of deoxynucleotide arrangements, the double helical structure, or the complex supercoiled spatial structure. Therefore, when designing a DNA molecule, priority is given to the order in which the bases are ordered, as well as to molecular thermal stability. NUPACK, developed by Caltech scholars, focuses on the analysis and design of nucleic acid systems, involving the secondary structure of nucleic acids for systems with one or more interacting strands [26]. According to this principle, we had designed three single stranded DNAs (C-apt, Hp1 and Hp2) in table I. These single strands were obtained by NUPACK design module [27] and then slightly modified according to their biological characteristics. Among them, aptamer sequences capable of specific binding to acetamiprid (5'-TGTA$_2$T$_3$GTCTGCAGCG$_2$T$_2$CT$_2$GATCGC TGACAC$_2$ATAT$_2$ATGA$_2$GA-3', named as S18) were first discovered by Liu and colleagues in 2011. And a 20-nt sequence (CTGACAC$_2$ATAT$_2$ATGA$_2$GA) at the loop3 of S18 was predicted to be the "target binding region" of acetamiprid and has been widely used in the determination of acetamiprid [28], [29].

TABLE I
THE DNA SEQUENCES USED IN THE EXPERIMENTS

Name	Sequence
Apt	CTGACACCATATTATGAAGA
C-apt	AGTCAGTGTGGATATGGTGTCAG
Hp1	CTGACACCATATCCACACTGACTCGGGTAGG GCGAGTCAGTGTGG
Hp2	CTGACTCGCCCTACCCGAGTCAGTGTGGCGG GTAGGGCGGGTTGGG

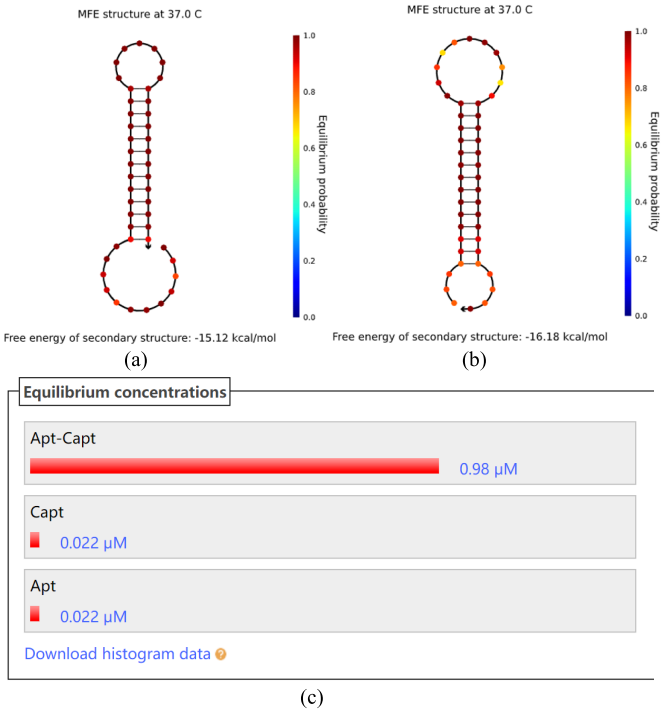

Fig. 2. Simulation results with NUPACK. (a) Simulation result of MFE structure at 37°C of Hp1. (b) Simulation result of MFE structure at 37°C of Hp2. (c) Equilibrium concentrations of Apt and C-apt.

For a given DNA sequence, calculations use dynamic programming [30] to compute a partition function, equilibrium base pair probability, and MFE(Minimum Free Energy) structure for each ordered complex based on thermodynamic studies of the secondary structure of nucleic acids [31]. Thus the Hp1 and Hp2 stem loop structures in the present model agree with our expectations and have low minimum free energies. As shown in Fig.2(a) and (b), F(Hp1) = −15.12kcal/mol, F(Hp2) = −16.18kcal/mol. The lower the free energy the more stable the structure, which indicated the theoretical feasibility of the structural sequence design of the two hairpins [32]. For calculations in which the maximum complex size is greater than one, the calculated partition functions and user-provided strand concentrations are used to calculate the equilibrium concentration of each ordered complex by solving

a convex optimization problem. Here in equilibrium, as shown in Fig. 2(c), the concentration of aptamer Apt and C-apt paired duplex is much higher than the respective single stranded concentration, reaching 98%, which is in accordance with the experimental expectation.

C. Verification of Feasibility by Computer Simulation

Visual DSD is a programming language and software tool for designing computing devices made of DNA with extensive modeling and analysis capabilities [33]. Simulation experiments are able to help us to pre judge the feasibility of the experiments and to initially determine the conditions for subsequent experiments, resulting in a reduction of the large amount of testing effort and saving time costs, human resources and expensive reagent supplies. The simulation algorithm framework of the detection process is as follows:

Input: ace
Output: fluorescence
  For i = 1, . . ., int(ace) **do**
    duplex ← Annealing(apt,c-apt);
    tp, ace/apt ← Addressing (ace);
    While(h1>0 or h2>0)
      tp/h1 ← Hybirdization(tp, h1);
      h1/h2, tp ← Hybirdization(tp/h1, h2);
      NMM(i) ← Signal(h1/h2);
    End while
  End for
  sNMM ← sum(NMM);
  NMM0 ← Leakage(c-apt)+Leakage(h1)+Leakage(h2);
  If (sNMM > NMM0)
    fluorescence ← true;
  Else
    fluorescence ← false;
  End if
End

And the obtained reaction process diagram of DNA machine is shown in Fig. 3. Thickened black boxes indicate input, with strands inside being initial reactants; sp indicates intermediate product; output indicates output of final product. Each number represents a stretch of base sequence, and the band * number indicates the sequence complementary to the base, such as <1> and <1*> are base complementary. The ends of the open arrows in the gray lines point to the products of the forward reaction, whereas the ends of the solid arrows represent the products of the reverse reaction. First, to facilitate computer input, the target acetamiprid was represented with a base sequence capable of complementary to the aptamer base, named ace. In theory, acetamiprid can specifically bind to the aptamer sequence in the duplex, releasing the trigger strand, which is denoted by tp. Next, the toehold region <2* > of the free tp strand is able to recognize and bind to the toehold <2> region exposed at the 5 'end of the hairpin h1, which in turn undergoes branch migration and gradually opens up the stem loop structure of h1, eventually combining the two strands to form the intermediate product duplex sp9. In the same way, the exposed toehold region <3*> in sp9 is able to bind to <3> of hairpin h2, which in turn completely displaces the ssDNA tp based on the strand displacement reaction and catalytic hairpin

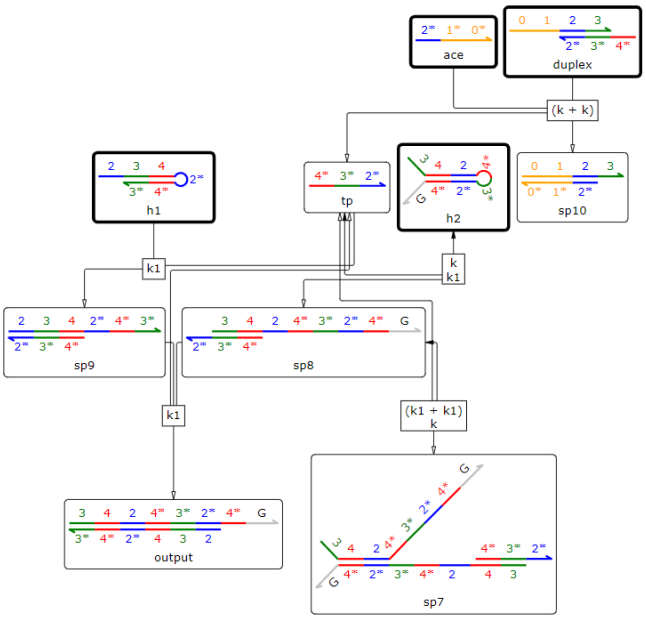

Fig. 3. DNA reaction process diagram of the developed strategy.

self-assembly and gives us the desired output complex of h1 and h2, where the exposed <4*G> contains enough guanine to form a G-quadruplex structure. Sp8 and sp7, as additional products, are likewise containing naked <4*g> fragments that can form G- quadruplex, and sp8 and sp9 also produce the product output we expect by undergoing strand displacement reactions through exposed toehold regions <2>, so there will be no false impact on the experiment.

Computer simulation experiments can also help us to clearly observe the content changes of individual chains as shown in Fig. 4. In the presence of the target, acetamiprid (blue line) is continuously consumed, and the trigger strand C-apt is released to constantly trigger the strand displacement reaction, and then the chain was completely replaced. It is shown in the figure that the content of the chain goes down after a short rise and then levels off, and finally the content rises to a plateau. Hairpins h1 (red line) and h2 (green line) are continuously consumed with decreasing contents up to a value of 0, and thus the duplex structures (orange line) composed of h1 and h2 show an upward trend and finally level off. In contrast, the individual reactant contents did not change appreciably in the absence of target, indicating that no expected product was produced. As can be seen above, the experimental principles devised are theoretically capable of achieving the purpose of the experiment.

D. Verification of Feasibility by Biological Experiments

In order to further verify the detection mechanism, polyacrylamide gel electrophoresis (PAGE) was also carried out. As shown in Fig. 5, the single clear bands contained in the first five lanes indicate single stranded Apt, single stranded C-apt, duplex C-apt/Apt, hairpin Hp1, hairpin Hp2, respectively, in which the number of bases in the duplex is slightly less than that in hairpin Hp1, so only slight differences can be seen. The lane 6 contains hairpins Hp1 and Hp2, so the band is a little deeper in color. The lane 7 contained trigger strand C-apt,

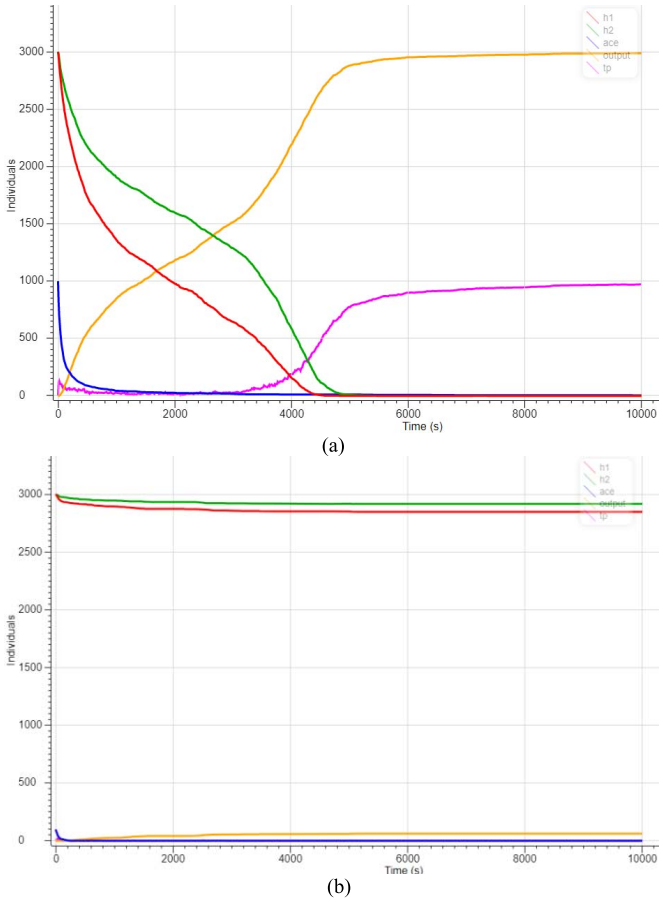

Fig. 4. Visual DSD simulations. The change in the number of strands over time in the system with acetamiprid (a), without acetamiprid (b).

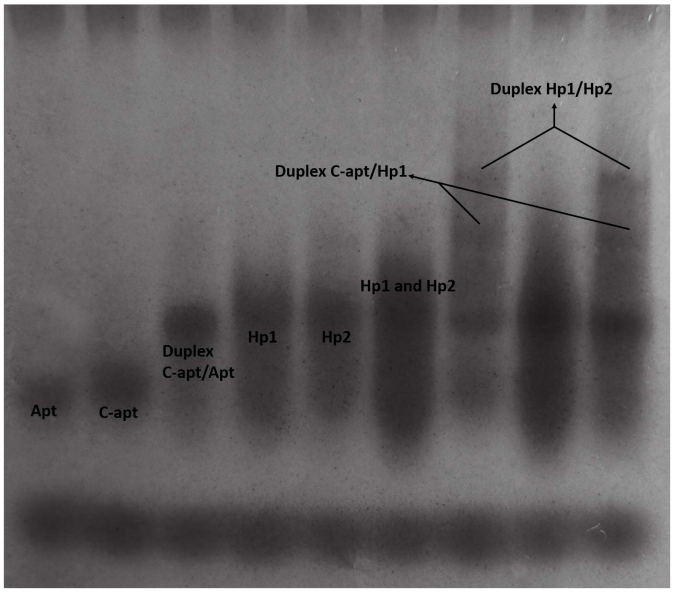

Fig. 5. Gel electrophoresis analysis. The concentrations of Ace, Apt, C-apt, C-apt/Apt, Hp1, and Hp2 were 500nM, 5μM, 5μM, 5μM, 5μM, and 5μM, respectively.

hairpin Hp1 and Hp2, and a new band appeared, the upper one shifted significantly slower than the others, indicating the production of the target product duplex Hp1/Hp2, and the middle one should be the intermediate product C-apt/Hp1, indicating

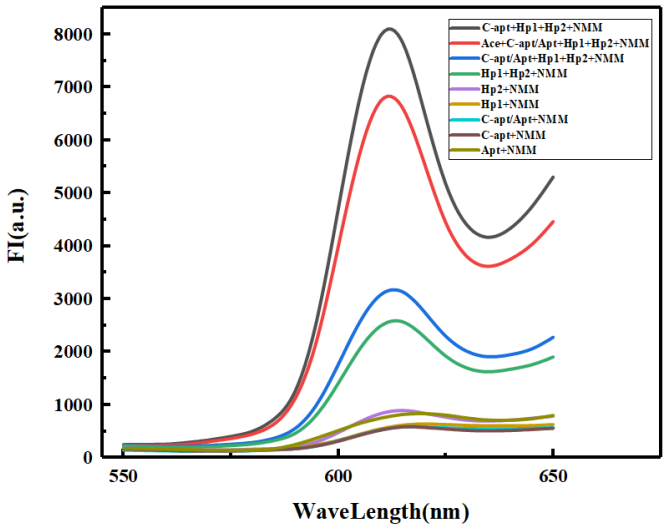

Fig. 6. Fluorescence spectra of NMM with different substances. The concentrations of Ace, C-apt, C-apt/Apt, Hp1, Hp2, and NMM were 100nM, 100nM, 100nM, 300 nM, 300 nM, and 2.0 μM, respectively.

the process by which the trigger strand opens hairpin Hp1. The lane 8, which contained the duplex C-apt/Apt, hairpins Hp1 and Hp2, did not generate new bands, indicating that Hp1 and Hp2 did not hybridize in the absence of the target acetamiprid. The lane 9, which contained the target acetamiprid, duplex C-apt/Apt, hairpins Hp1 and Hp2, similar to the lane 7, also generated new bands, demonstrating the feasibility of this strategy.

To further demonstrate the feasibility of the proposed strategy, the fluorescence intensity under various conditions was experimentally verified as shown in Fig. 6. When the solution contains only Apt, C-apt, duplex C-apt/Apt, Hp1, or Hp2 (corresponding to the bottom five lines, respectively), the fluorescence intensity was very low and essentially no fluorescence signal was generated. When the reactants had only Hp1 and Hp2, only less intense fluorescent bands (green) were produced. However the increase of fluorescence intensity at 610 nm (black) was obviously seen when the trigger strand C-apt was added to the mixture. When only the target is absent, the intact DNA machine contains the double strand and the two hairpins and also produces only a less intense fluorescent band, but a slightly higher relative green fluorescent band due to possible leakage from the double stranded structure, resulting in an increase in background fluorescence (blue). Upon addition of the target acetamiprid, the fluorescence intensity was obviously enhanced (red) than that of the system without the target, but slightly lower than that of directly adding the trigger strand, because the reaction process of the target with the duplex takes time and no complete reaction exists. In conclusion, there was an obvious change in the fluorescence intensity between the spiked target and the unloaded target, which was able to demonstrate the feasibility of the strategy.

E. Optimization of Acetamiprid Detection Conditions

Considering that the preparation of double strands is involved in the proposed strategy, it is critical to optimization of the ratio of Apt and C-apt if the C-apt is in excess, the

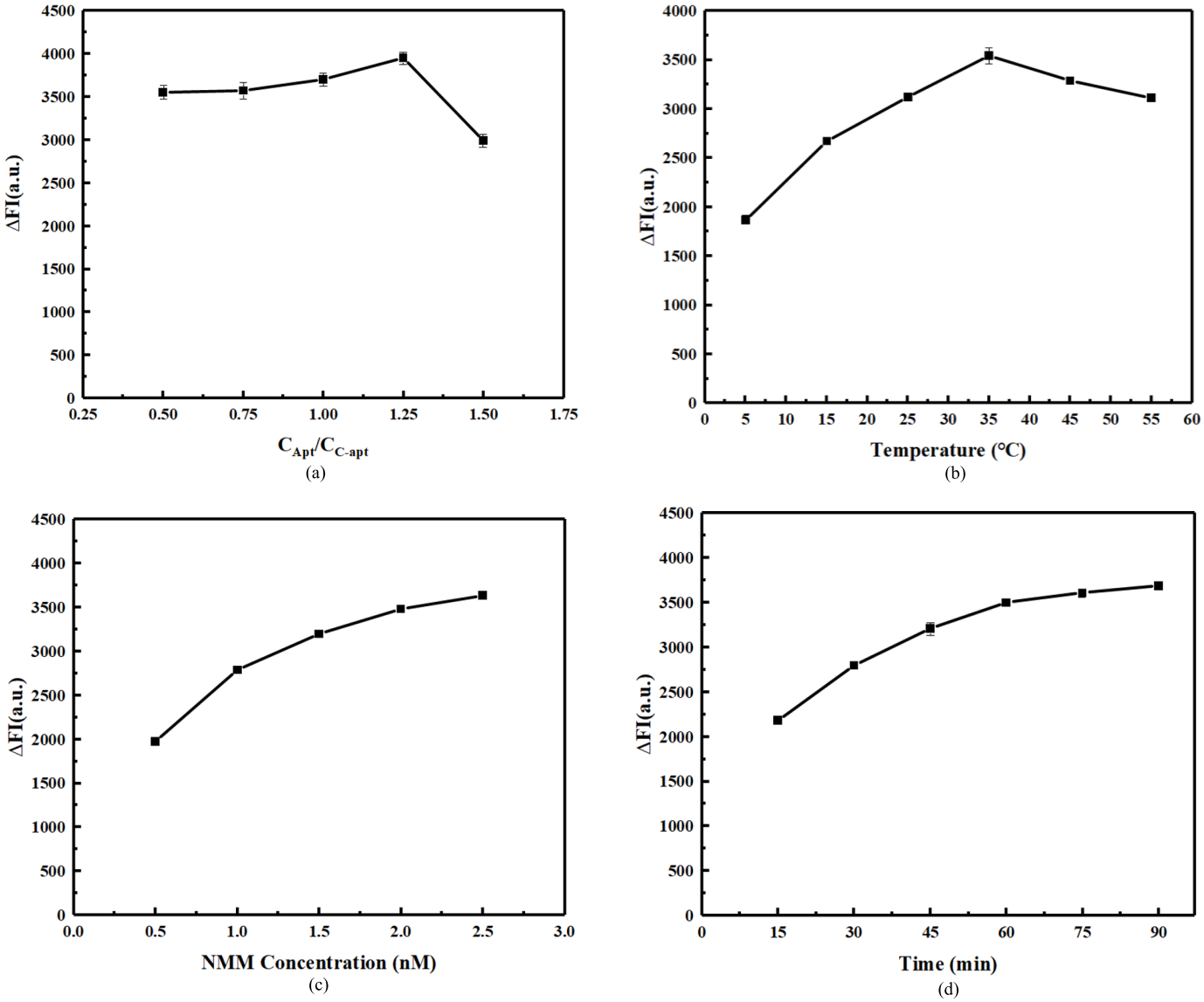

Fig. 7. Plots were optimized for the ratio of Apt to C-apt (a), temperature (b), NMM concentration (c), time (d) conditions, and error bars represent triplicate trials.

DNA machinery, in the absence of the target, also triggers subsequent reactions, leading to false positive feedback results. If the Apt is in excess, more acetamiprid is needed to initiate the DNA machinery, leading to a decrease in sensitivity. To ensure more sufficient binding of Apt and C-apt, the concentration of C-apt was first fixed at 100 nM, and then the concentration of the added Apt was gradually changed, followed by 50 nM, 75 nM, 100 nM, 125 nM, 150 nM. SYBR Green was chosen as a signal reporter for duplex formation because it fluoresces upon binding to the duplex and the fluorescence intensity and number of DNA duplexes is positively correlated. As illustrated in Fig. 7(a), the fluorescence intensity increased with the addition of Apt, which indicated that the number of double strands increased. The fluorescence intensity reached a maximum at the ratio of Apt to C-apt of 1.25:1, which illustrated that Apt and C-apt reacted most thoroughly at this ratio, and this result was also used in subsequent experiments.

The effect of temperature on the experimental process was expressed as follows: when the temperature was too high, the hairpin structure was unstable leading to abnormal experimental results, and when the temperature was too low, the hairpin structure was too stable leading to too retarded reaction. Therefore, it is also crucial to choose the optimal experimental temperature. Either too low or too high a temperature, as shown in Fig. 7(b), did not work well for the DNA machine and was optimal at 35°C, and the results were also derived for subsequent experiments.

As shown in Fig. 7(c), when the concentration of NMM is 2 μM, the detection performance is the best. Low concentration of NMM is not enough to provide the fluorescence signal of G-quadruplex, while high concentration of NMM will increase the background fluorescence and reduce the sensitivity. So it is very important to choose the optimal concentration of NMM for our experiment. The optimized results are also used in subsequent experiments.

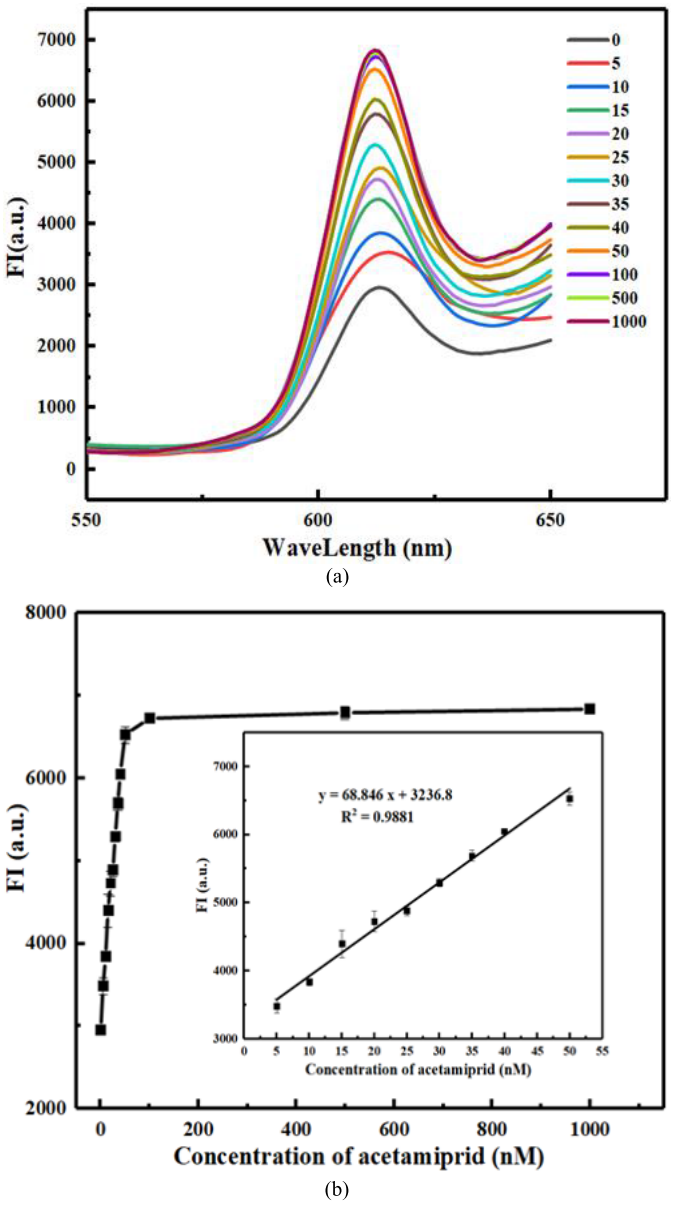

Fig. 8. Fluorescence spectra after adding different concentrations of acetamiprid (a), Fluorescence intensity values of different concentrations of acetamiprid (b). The inset shows the linear relationship between acetamiprid concentration and fluorescence intensity in the response range of 0∼50nM. Error bars represent triplicate trials.

Finally, the incubation times of the experiments were also investigated, as shown in Fig. 7(d). In the first 75 min, the fluorescence intensity of G-quadruplex gradually increased. When the incubation time continued to be extended, no obvious fluorescence enhancement occurred, which suggested that the strand displacement and catalytic hairpin self-assembly reactions in the system had been relatively thorough.

F. Analytical Performance of Acetamiprid Assay

To examine the analytical performance of the developed sensor for Acetamiprid in aqueous solution, the fluorescence intensity in the system containing different concentrations of acetamiprid was measured under the optimized conditions. Results as shown in Fig. 8(a), the fluorescence intensity increased rapidly as the concentration of acetamiprid increased from 5 nM to 50 nM. This indicated that more and more G-quadruplex were formed as the concentration of acetamiprid added increased, and thus had a stronger fluorescence effect. After the concentration of acetamiprid was further added to 100 nM, the fluorescence intensity of the system had no obvious change. From these increases in fluorescence signal, the level of acetamiprid can be estimated. Fig. 8(b) depicts the relationship of fluorescence intensity with the concentration of acetamiprid, exhibiting a very good linear relationship in the range of 5-50 nM with a correlation coefficient of 0.9881. A detection limit of 54.3 pM was estimated with a 3-fold definition of the standard deviation of the blank / slope. Table II lists the limits of detection of acetamiprid in other analytical methods. Most of these analytical methods have high detection limits relative to our proposed strategy, and may involve expensive materials or complicated operations.

To verify whether the experimental protocols had the same performance under complex conditions, two common fruits (Apple) and vegetables (Chinese cabbage) were selected as real samples and pretreated. A known standard solution of acetamiprid was added to the sample solution for spiked recovery test. Table III shows that the recoveries obtained from three repeated experiments are in the range of 97.6-105.2%, indicating that the accuracy and reproducibility of this acetamiprid detection method make it promising in the field of food safety.

TABLE II
COMPARISON OF THE DETECTION METHOD IN THIS ARTICLE WITH OTHER RESEARCH METHODS

Detection methods	Linear ranger (nM)	LOD (nM)
High-performance liquid chromatography (HPLC) [34]	/	44.9
Liquid chromatography tandem mass spectrometry (LCMS/MS) [35]	4.49 - 4490	1.3
Photoelectrochemical aptasensor[36]	/	0.180
Multiple complementary strands (CSs), and AuNPs Fluorometry[37]	5 - 50	2.8
Aptamerconjugated magnet nanoparticles and complementary DNA-conjugated UCNPs[38]	3.9 - 513	2.9
G-quadruplex/hemin DNAzyme, and graphene quantum dots functionalized with D-penicillamine and histidine[39]	0.000001-1.0	0.00000038
ZnS:Mn QDs[40]	0–150	0.07
This work	5 - 50	0.0543

TABLE III
DETERMINATION OF ACETAMIPRID SPIKED IN APPLE AND CHINESE CABBAGE EXTRACT SAMPLES

Sample	Added (nM)	Detected(nM)	Recovery(%)
Apple	5	5.26	105.20
	20	20.56	102.80
	50	49.98	99.96
Chinese cabbage	5	5.09	101.80
	20	19.52	97.60
	50	50.30	100.60

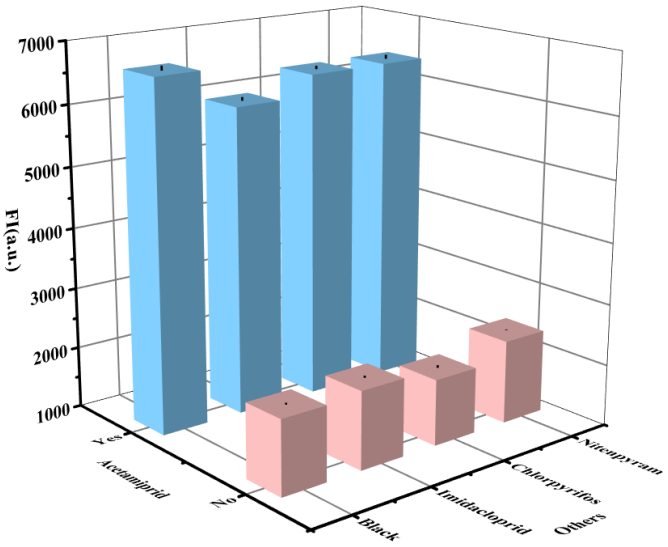

Fig. 9. The specificity and interference experiment of acetamiprid detection. The concentration of acetamiprid was 100 nM, and the other pesticides were used with the concentration of 500 nM. Error bars represent triplicate trials.

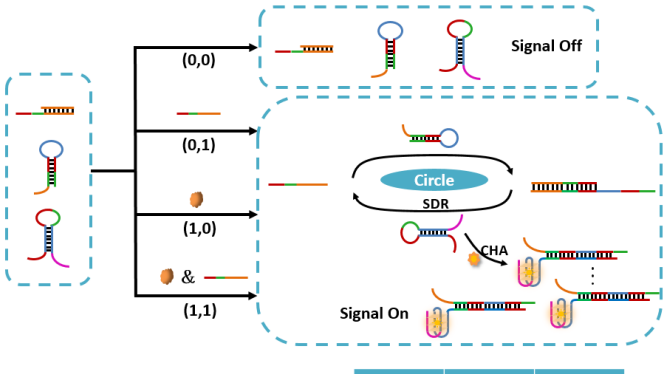

Input1	Input2	Output
0	0	0
0	1	1
1	0	1
1	1	1

Fig. 10. Design principle, logic symbol and truth table of OR logic gate.

In addition, several pesticides commonly used in life were selected to evaluate the anti-interference ability of this fluorescence detection method, including chlorpyrifos, imidacloprid and nitenpyram. Among them, imidacloprid and nitenpyram, similar to acetamiprid, belong to neonicotinoid pesticides and chlorpyrifos to organophosphorus pesticides. As can be seen from Fig. 9, a strong fluorescence signal could be detected only for the sample containing acetamiprid, demonstrating the good specificity of this method. And other types of insecticides do not affect this detection means and have good anti-interference ability.

G. Construction and Simulation Verification of Basic Logic Gates

This strategy is also beneficial for constructing molecular logic gates due to the advantages of enzyme-free, label-free and high stability of DNA strand reaction, which provide ideas for implementing complex logic operations. After the rational design of analytes and fluorescence signals, the basic bio logic gates, including the OR gate and the AND gate, were constructed. Here, the target and C-apt were used as the two

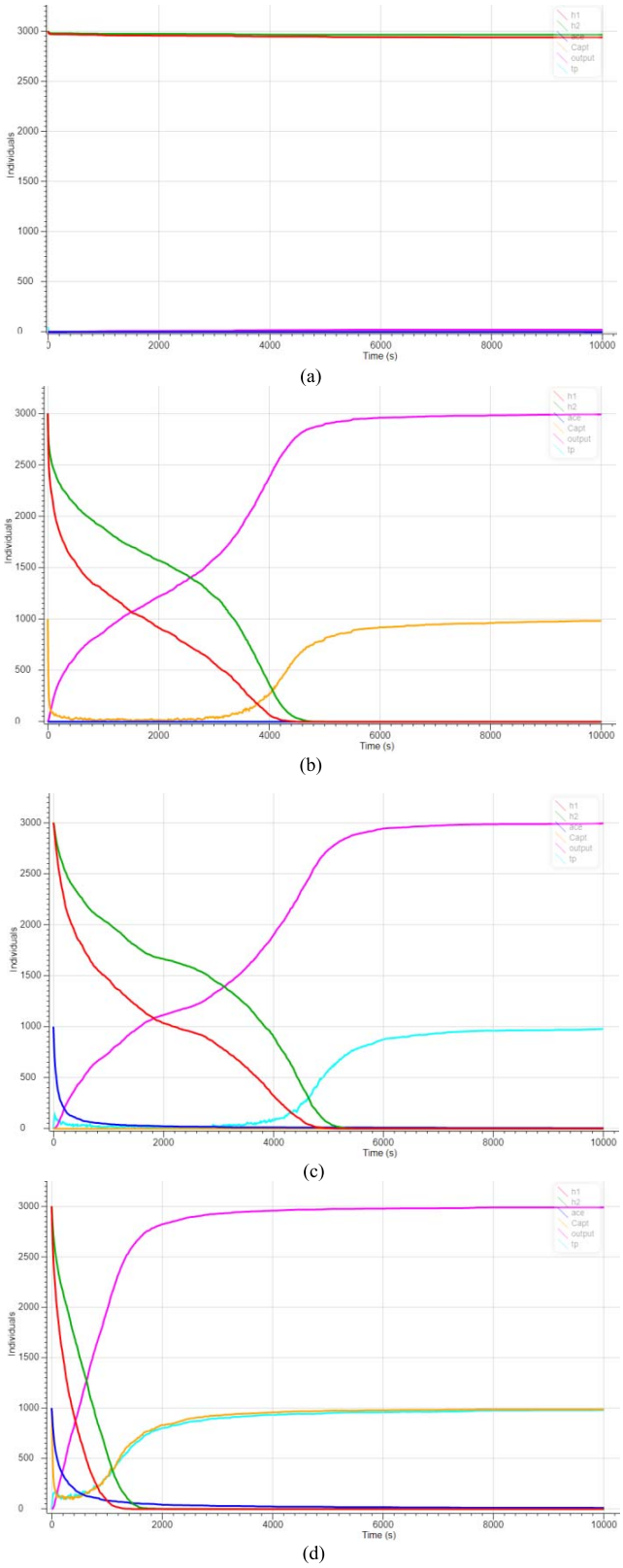

Fig. 11. Visual DSD simulation of the OR logic gate. (a), (b), (c), and (d) represent the time-dependent curves of reactants and products during the reaction when the inputs are (0,0), (0,1), (1,0) and (1,1).

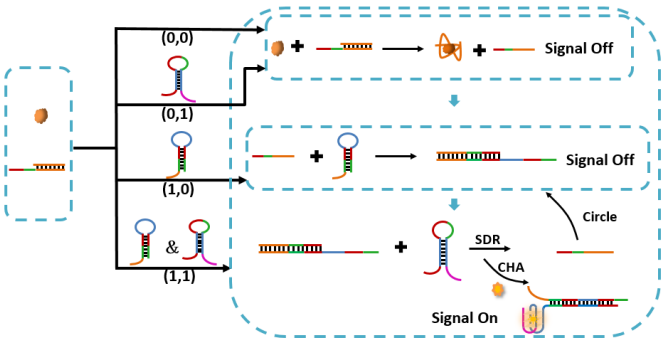

Input1	Input2	Output
0	0	0
0	1	0
1	0	0
1	1	1

Fig. 12. Design principle, logic symbol and truth table of AND logic gate.

inputs of the OR gate, the strong fluorescence signal as the output 1, and the weak fluorescence signal as the output 0. The input of either presence triggers a subsequent reaction, producing a complex of Hp1 and Hp2, and a fluorescence signal under the action of NMM, that is, (0,1), (1,0), and (1,1) case. While both inputs are zero, the expression of the subsequent reaction cannot be triggered and the fluorescence signal is not expressed. Fig. 10 shows a schematic representation, truth table and circuit symbols of the OR gate.

Next, the reaction was monitored by visual DSD to verify the implementation of the OR logic gate. As shown in Fig. 11(a), (b), (c), and (d) in turn are plots of the amounts of the respective reactants and products as a function of time in the (0,0), (0,1), (1,0), and (1,1) cases. When there is neither target(ace, blue) nor trigger chain(Capt, yellow), the content of each reactant is basically unchanged, and there is no target product(output, pink); In the case of only trigger chain and only target, the change of reactant content is basically the same, producing a large number of target product, and reaching equilibrium at about 5000s; In the case of both target and trigger chain, the time required to reach the equilibrium state is almost halved, because both can trigger the subsequent reaction.

As shown in Fig. 12, a schematic diagram of the AND gate, Hp1 and Hp2 are used as the two inputs for the logic operation, and the fluorescence signal is similarly used as the output signal. It can be seen from the figure that when the input is (0, 0) and (0, 1), the reaction process is the same, and only the first step can occur to obtain the trigger strand C-apt, and the subsequent reaction cannot occur due to the absence of hairpin Hp1; When the input is (1, 0), the trigger strand generated after the target binds to the aptamer can continue to react with Hp1 to produce the duplex C-apt/Hp1; When the input is (1,1), the reaction occurs completely, producing double stranded Hp1/Hp2, and resulting in a fluorescence signal under the action of NMM. The logical symbols and truth tables are also shown in Fig. 12.

The reaction process simulation of the AND logic gate in four different input states is shown in Fig. 13. When both inputs are 0, single chain tp (light blue) is generated; When there is only Hp2, there is one more strip (h2, green) representing Hp2 than when the input is (0,0); When there is only Hp1, the generated tp will open Hp1 and form a double chain

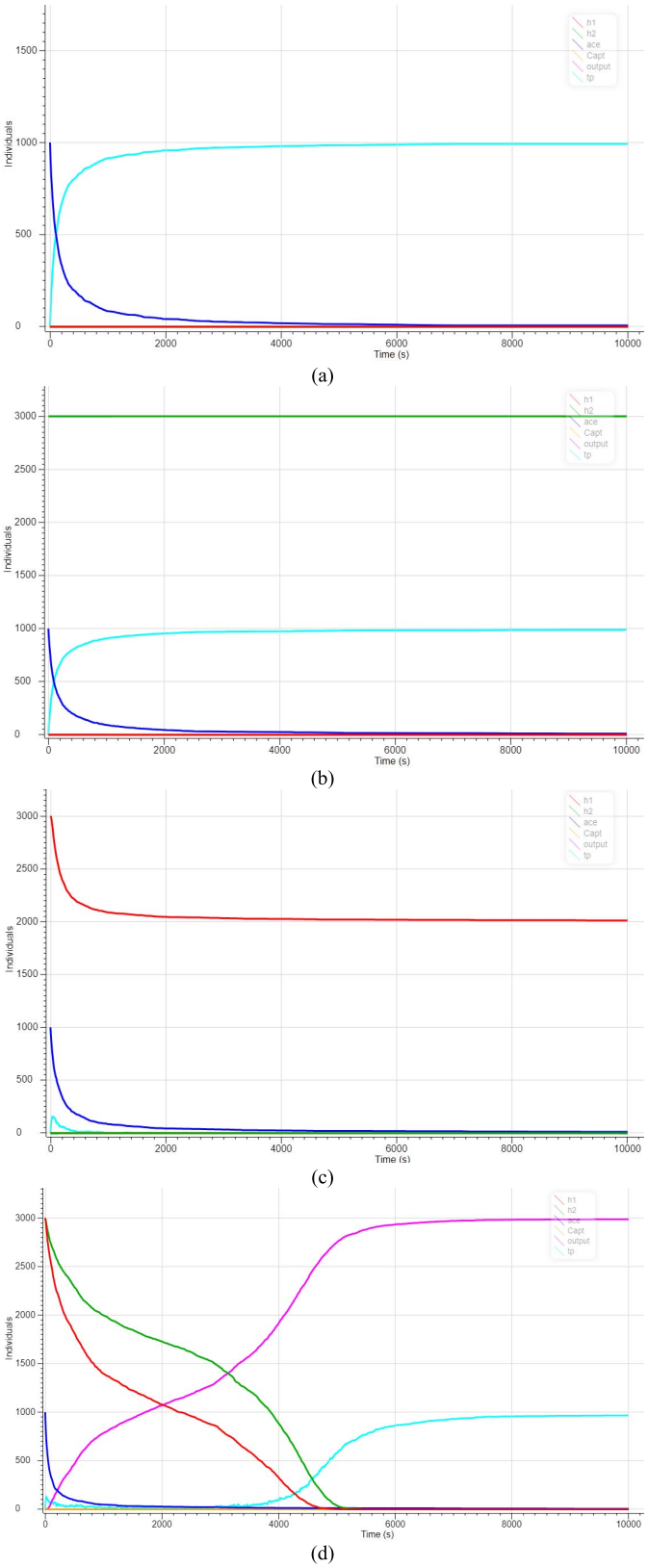

Fig. 13. Visual DSD simulation of the AND logic gate. (a), (b), (c), and (d) represent the time-dependent curves of reactants and products during the reaction when the inputs are (0,0), (0,1), (1,0), and (1,1).

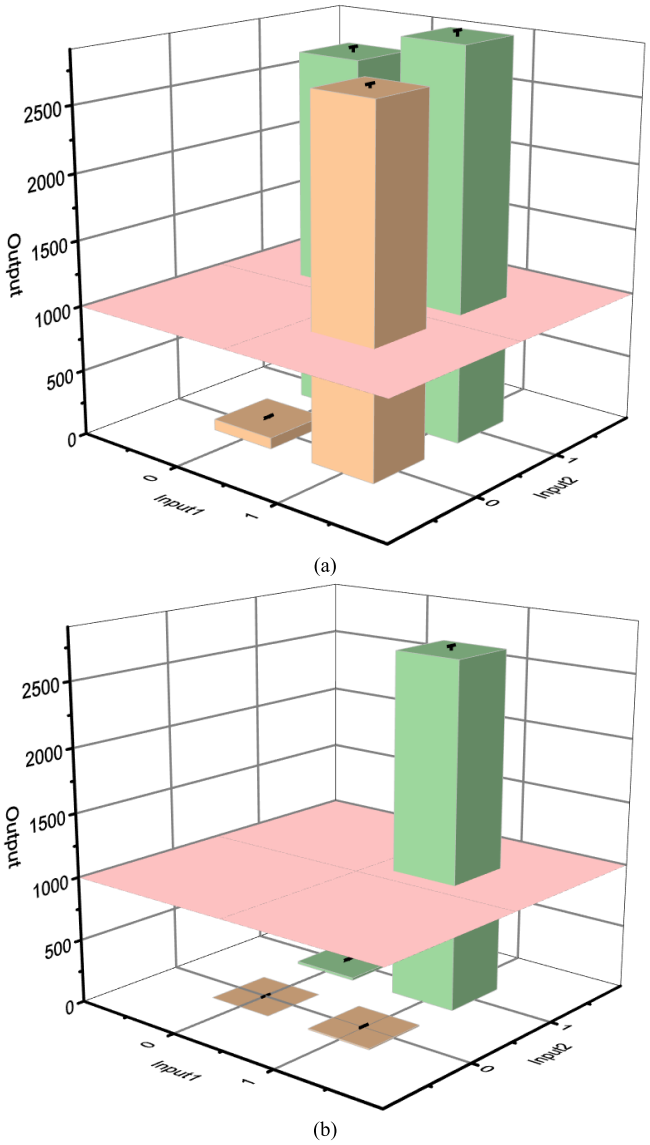

Fig. 14. Analysis of logical results of OR gate (a) and AND gate (b), and error bars represent triplicate trials.

structure, so tp bands are basically consumed, while Hp1(hp1, red) are reduced to equilibrium, and the amount of reduction is basically equal to the amount of tp generated; In the presence of both Hp1 and Hp2, it can be seen from the figure that a large number of target product double chain Hp1/Hp2 are produced, that is, the output band (pink) gradually increases to equilibrium.

The amount of target product at 4000s was taken as the judge of the logic gate function, with higher than threshold representing the output as 1 and lower than threshold representing the output as 0. The results are shown in Fig. 14, with the OR gate (a) and the AND gate (b), and the threshold was set as 1000. Combining the results of the comparative simulation experiment and the fluorescence biological experiment, the fluorescence threshold was chosen to be 4000, and the reaction time was 5000s. The results of three repeated logic experiments were shown in table IV. It is obvious from the table that the output of both OR gate and AND gate correspond to their truth tables, demonstrating the feasibility of using this strategy to construct the underlying logic components.

TABLE IV
DETERMINATION OF ACETAMIPRID SPIKED IN APPLE AND CHINESE CABBAGE EXTRACT SAMPLES

Logic mate	Input	FI(a.u.)	Output
OR	(0,0)	2383	0
	(0,1)	7021	1
	(1,0)	6854	1
	(1,1)	7947	1
AND	(0,0)	609	0
	(0,1)	969	0
	(1,0)	854	0
	(1,1)	6902	1

IV. CONCLUSION

In summary, an enzyme-free and label-free DNA biosensor for acetamiprid detection was developed based on strand displacement reaction and catalytic hairpin self-assembly technology, and the feasibility of this strategy was verified by computer simulation and biological experiments. After optimization, a good linear relationship was obtained in the range of 5-50 nM, and a detection limit of 54.3 pM was calculated. And by setting different inputs, a logic computing platform including OR gate and AND gate is constructed. The operability is verified by simulation experiments and biological experiments. Pre experimental computer simulation makes subsequent biological experiments more directed and simplifies the experimental flow; Second, the proposed strategy has no involvement of enzymes and does not require labeling fluorophores and quenching groups, making the experimental manipulation simple and having good economic benefits and also making the logic gate not overly dependent on confined environmental conditions; Finally, this strategy is ingeniously designed with a trigger mechanism and a probe signal hidden in the hairpin, so it can serve as a good general platform for sensing and Computing.

REFERENCES

[1] P. Weerathunge, R. Ramanathan, R. Shukla, T. K. Sharma, and V. Bansal, "Aptamer-controlled reversible inhibition of gold nanozyme activity for pesticide sensing," *Anal. Chem.*, vol. 86, no. 24, pp. 11937–11941, Dec. 2014, doi: 10.1021/ac5028726.

[2] L. Fan, G. Zhao, H. Shi, M. Liu, and Z. Li, "A highly selective electrochemical impedance spectroscopy-based aptasensor for sensitive detection of acetamiprid," *Biosensors Bioelectron.*, vol. 43, pp. 12–18, May 2013, doi: 10.1016/j.bios.2012.11.033.

[3] H. Shi, G. Zhao, M. Liu, L. Fan, and T. Cao, "Aptamer-based colorimetric sensing of acetamiprid in soil samples: Sensitivity, selectivity and mechanism," *J. Hazardous Mater.*, vol. 260, pp. 754–761, Sep. 2013, doi: 10.1016/j.jhazmat.2013.06.031.

[4] R. Rapini, A. Cincinelli, and G. Marrazza, "Acetamiprid multidetection by disposable electrochemical DNA aptasensor," *Talanta*, vol. 161, pp. 15–21, Dec. 2016, doi: 10.1016/j.talanta.2016.08.026.

[5] S. D. Gomez, P. S. Bustos, V. G. Sánchez, M. G. Ortega, and N. Guiñazú, "Trophoblast toxicity of the neonicotinoid insecticide acetamiprid and an acetamiprid-based formulation," *Toxicology*, vol. 431, Feb. 2020, Art. no. 152363, doi: 10.1016/j.tox.2020.152363.

[6] J. Liu, F. Zhao, Y. Xu, J. Qiu, and Y. Qian, "Gut flora-mediated metabolic health, the risk produced by dietary exposure to acetamiprid and tebuconazole," *Foods*, vol. 10, no. 4, p. 835, Apr. 2021, doi: 10.3390/foods10040835.

[7] A. Y. Kocaman and M. Topaktas, "Genotoxic effects of a particular mixture of acetamiprid and α-cypermethrin on chromosome aberration, sister chromatid exchange, and micronucleus formation in human peripheral blood lymphocytes," *Environ. Toxicol.*, vol. 25, pp. 157–168, Apr. 2010, doi: 10.1002/tox.20485.

[8] A. Y. Kocaman and M. Topaktaş, "*In vitro* evaluation of the genotoxicity of acetamiprid in human peripheral blood lymphocytes," *Environ. Mol. Mutagenesis*, vol. 48, no. 6, pp. 483–490, Jul. 2007, doi: 10.1002/em.20309.

[9] W. Han, Y. Tian, and X. Shen, "Human exposure to neonicotinoid insecticides and the evaluation of their potential toxicity: An overview," *Chemosphere*, vol. 192, pp. 59–65, Feb. 2018, doi: 10.1016/j.chemosphere.2017.10.149.

[10] A. Fei *et al.*, "Label-free impedimetric aptasensor for detection of femtomole level acetamiprid using gold nanoparticles decorated multiwalled carbon nanotube-reduced graphene oxide nanoribbon composites," *Biosensors Bioelectron.*, vol. 70, pp. 122–129, Aug. 2015, doi: 10.1016/j.bios.2015.03.028.

[11] T. Kuretake, S. Kawahara, M. Motooka, and S. Uno, "An electrochemical gas biosensor based on enzymes immobilized on chromatography paper for ethanol vapor detection," *Sensors*, vol. 17, no. 2, p. 281, Feb. 2017, doi: 10.3390/s17020281.

[12] W. Xie, C. Han, Y. Qian, H. Ding, X. Chen, and J. Xi, "Determination of neonicotinoid pesticides residues in agricultural samples by solid-phase extraction combined with liquid chromatography–tandem mass spectrometry," *J. Chromatogr. A*, vol. 1218, no. 28, pp. 4426–4433, Jul. 2011, doi: 10.1016/j.chroma.2011.05.026.

[13] S. Wanatabe *et al.*, "Development of competitive enzyme-linked immunosorbent assays (ELISAs) based on monoclonal antibodies for chloronicotinoid insecticides imidacloprid and acetamiprid," *Anal. Chim. Acta*, vol. 427, no. 2, pp. 211–219, 2001, doi: 10.1016/S0003-2670(00)01126-0.

[14] I. S. de Murieta and A. Rodríguez-Patón, "DNA biosensors that reason," *Biosystems*, vol. 109, pp. 91–104, Aug. 2012, doi: 10.1016/j.biosystems.2012.02.005.

[15] L. Qian and E. Winfree, "Scaling up digital circuit computation with DNA strand displacement cascades," *Science*, vol. 332, no. 6034, pp. 1196–1202, 2011, doi: 10.1126/science.1200520.

[16] Y. Zhang *et al.*, "A simple electrochemical biosensor for highly sensitive and specific detection of microRNA based on mismatched catalytic hairpin assembly," *Biosensors Bioelectron.*, vol. 68, pp. 343–349, Jun. 2015, doi: 10.1016/j.bios.2015.01.026.

[17] D. Li *et al.*, "Catalytic hairpin assembly actuated DNA nanotweezer for logic gate building and sensitive enzyme-free biosensing of MicroRNAs," *Anal. Chem.*, vol. 88, no. 15, pp. 7500–7506, Aug. 2016, doi: 10.1021/acs.analchem.5b04844.

[18] X. Gong, J. Wei, J. Liu, R. Li, X. Liu, and F. Wang, "Programmable intracellular DNA biocomputing circuits for reliable cell recognitions," *Chem. Sci.*, vol. 10, no. 10, pp. 2989–2997, Mar. 2019, doi: 10.1039/C8SC05217D.

[19] P. Miao and Y. Tang, "Cascade strand displacement and bipedal walking based DNA logic system for miRNA diagnostics," *ACS Central Sci.*, vol. 7, no. 6, pp. 1036–1044, Jun. 2021, doi: 10.1021/acscentsci.1c00277.

[20] H. T. Baytekin and E. U. Akkaya, "A molecular NAND gate based on Watson–Crick base pairing," *Organic Lett.*, vol. 2, no. 12, pp. 1725–1727, Jun. 2000, doi: 10.1021/ol005873c.

[21] Y. Chen, S.-H. Lee, and C. Mao, "A DNA nanomachine based on a duplex–triplex transition," *Angew. Chem. Int. Ed.*, vol. 43, no. 40, pp. 5335–5338, Oct. 2004, doi: 10.1002/anie.200460789.

[22] M. R. Lakin, S. Youssef, F. Polo, S. Emmott, and A. Phillips, "Visual DSD: A design and analysis tool for DNA strand displacement systems," *Bioinformatics*, vol. 27, no. 22, pp. 3211–3213, 2011, doi: doi:10.1093/bioinformatics/btr543.

[23] M. K. Beissenhirtz and I. Willner, "DNA-based machines," *Org. Biomol. Chem.*, vol. 4, no. 18, pp. 3392–3401, 2006, doi: 10.1039/b607033g.

[24] J. M. Nicoludis *et al.*, "Optimized end-stacking provides specificity of N-methyl mesoporphyrin IX for human telomeric G-quadruplex DNA," *J. Amer. Chem. Soc.*, vol. 134, no. 50, pp. 20446–20456, Dec. 2012, doi: 10.1021/ja3088746.

[25] L. Guo *et al.*, "A G-quadruplex based label-free fluorescent biosensor for lead ion," *Biosensors Bioelectron.*, vol. 35, no. 1, pp. 123–127, May 2012, doi: 10.1016/j.bios.2012.02.031.

[26] J. N. Zadeh *et al.*, "NUPACK: Analysis and design of nucleic acid systems," *J. Comput. Chem.*, vol. 32, no. 1, pp. 170–173, Jan. 2011, doi: 10.1002/jcc.21596.

[27] R. M. Dirks and N. A. Pierce, "An algorithm for computing nucleic acid base-pairing probabilities including pseudoknots," *J. Comput. Chem.*, vol. 25, no. 10, pp. 1295–1304, Jul. 2004, doi: 10.1002/jcc.20057.

[28] J. He, Y. Liu, M. Fan, and X. Liu, "Isolation and identification of the DNA aptamer target to acetamiprid," *J. Agricult. Food Chem.*, vol. 59, no. 5, pp. 1582–1586, Mar. 2011, doi: 10.1021/jf104189g.

[29] K. Fan, W. Kang, S. Qu, L. Li, B. Qu, and L. Lu, "A label-free and enzyme-free fluorescent aptasensor for sensitive detection of acetamiprid based on AT-rich dsDNA-templated copper nanoparticles," *Talanta*, vol. 197, pp. 645–652, May 2019, doi: 10.1016/j.talanta.2019.01.069.

[30] J. S. McCaskill, "The equilibrium partition function and base pair binding probabilities for RNA secondary structure," *Biopolymers*, vol. 29, nos. 6–7, pp. 1105–1119, May 1990, doi: 10.1002/bip.360290621.

[31] M. E. Fornace, N. J. Porubsky, and N. A. Pierce, "A unified dynamic programming framework for the analysis of interacting nucleic acid strands: Enhanced models, scalability, and speed," *ACS Synth. Biol.*, vol. 9, no. 10, pp. 2665–2678, Oct. 2020, doi: 10.1021/acssynbio.9b00523.

[32] Y. Zhang, L. Wang, Y. Wang, and Y. Dong, "Label-free optical biosensor for target detection based on simulation-assisted catalyzed hairpin assembly," *Comput. Biol. Chem.*, vol. 78, pp. 448–454, Feb. 2019, doi: 10.1016/j.compbiolchem.2018.11.030.

[33] W. Xiao, X. Zhang, Z. Zhang, C. Chen, and X. Shi, "Molecular full adder based on DNA strand displacement," *IEEE Access*, vol. 8, pp. 189796–189801, 2020, doi: 10.1109/ACCESS.2020.3031221.

[34] H. Obana, M. Okihashi, K. Akutsu, Y. Kitagawa, and S. Hori, "Determination of acetamiprid, imidacloprid, and nitenpyram residues in vegetables and fruits by high-performance liquid chromatography with diode-array detection," *J. Agricult. Food Chem.*, vol. 50, no. 16, pp. 4464–4467, Jul. 2002, doi: 10.1021/jf025539q.

[35] S. Song *et al.*, "Simultaneous determination of neonicotinoid insecticides and insect growth regulators residues in honey using LC–MS/MS with anion exchanger-disposable pipette extraction," *J. Chromatogr. A*, vol. 1557, pp. 51–61, Jul. 2018, doi: 10.1016/j.chroma.2018.05.003.

[36] H. Li, Y. Qiao, J. Li, H. Fang, D. Fan, and W. Wang, "A sensitive and label-free photoelectrochemical aptasensor using Co-doped ZnO diluted magnetic semiconductor nanoparticles," *Biosensors Bioelectron.*, vol. 77, pp. 378–384, Mar. 2016, doi: 10.1016/j.bios.2015.09.066.

[37] L. Yang, H. Sun, X. Wang, W. Yao, W. Zhang, and L. Jiang, "An aptamer based aggregation assay for the neonicotinoid insecticide acetamiprid using fluorescent upconversion nanoparticles and DNA functionalized gold nanoparticles," *Microchim. Acta*, vol. 186, no. 5, pp. 1–11, May 2019, doi: 10.1007/s00604-019-3422-9.

[38] N. Sun, Y. Ding, Z. Tao, H. You, X. Hua, and M. Wang, "Development of an upconversion fluorescence DNA probe for the detection of acetamiprid by magnetic nanoparticles separation," *Food Chem.*, vol. 257, pp. 289–294, Aug. 2018, doi: 10.1016/j.foodchem.2018.02.148.

[39] L. Nana, L. Ruiyi, S. Xiulan, Y. Yongqiang, and L. Zaijun, "Dual amplification in a fluorometric acetamiprid assay by using an aptamer, G-quadruplex/hemin DNAzyme, and graphene quantum dots functionalized with D-penicillamine and histidine," *Microchim. Acta*, vol. 187, no. 3, pp. 1–10, Mar. 2020, doi: 10.1007/s00604-020-4127-9.

[40] L. Zeng, D. Zhou, J. Wu, C. Liu, and J. Chen, "A target-induced and equipment-free biosensor for amplified visual detection of pesticide acetamiprid with high sensitivity and selectivity," *Anal. Methods*, vol. 11, no. 9, pp. 1168–1173, Feb. 2019, doi: 10.1039/c8ay02513d.